ADVANCES IN ATMOSPHERIC SCIENCES, VOL. 35, NOVEMBER 2018, 1381–1395

• **Original Paper** •

Influence of Atmospheric Particulate Matter on Ozone in Nanjing, China: Observational Study and Mechanistic Analysis

Yawei QU[1], Tijian WANG*[1], Yanfeng CAI[2], Shekou WANG[3], Pulong CHEN[1], Shu LI[1],
Mengmeng LI[1], Cheng YUAN[1], Jing WANG[4], and Shaocai XU[4]

[1] *School of Atmospheric Sciences, CMA-NJU Joint Laboratory for Climate Prediction Studies,*
Jiangsu Collaborative Innovation Center for Climate Change, Nanjing University, Nanjing 210023*, China*
[2] *Guangdong Electric Power Design Institution Co., Ltd. of China Energy Engineering Group, Guangzhou* 510663*, China*
[3] *Jiangsu Academy of Environmental Industry and Technology Crop, Nanjing* 210036*, China*
[4] *Qingdao Environmental Monitoring Center, Qingdao* 266003*, China*

(Received 27 January 2018; revised 21 May 2018; accepted 07 June 2018)

ABSTRACT

Particulate matter with diameters of 2.5 µm or smaller ($PM_{2.5}$) and ozone (O_3) are major pollutants in the urban atmosphere. $PM_{2.5}$ can affect O_3 by altering the photolysis rate and heterogeneous reactions. However, these two processes and their relative importance remain uncertain. In this paper, with Nanjing in China as the target city, we investigate the characteristics and mechanism of interactions between particles and O_3 based on ground observations and numerical modeling. In 2008, the average concentrations of $PM_{2.5}$ and O_3 at Caochangmen station are 64.6 ± 47.4 µg m^{-3} and 24.6 ± 22.8 ppb, respectively, while at Pukou station they are 94.1 ± 63.4 µg m^{-3} and 16.9 ± 14.9 ppb. The correlation coefficient between $PM_{2.5}$ and O_3 is -0.46. In order to understand the reaction between $PM_{2.5}$ and O_3, we construct a box model, in which an aerosol optical property model, ultraviolet radiation model, gas phase chemistry model, and heterogeneous chemistry model, are coupled. The model is employed to investigate the relative contribution of the aforementioned two processes, which vary under different particle concentrations, scattering capability and VOCs/NO_x ratios (VOCs: volatile organic compounds; NO_x: nitric oxide and nitrogen dioxide). Generally, photolysis rate effect can cause a greater O_3 reduction when the particle concentrations are higher, while heterogeneous reactions dominate O_3 reduction with low-level particle concentrations. Moreover, in typical VOC-sensitive regions, O_3 can even be increased by heterogeneous reactions. In Nanjing, both processes lead to O_3 reduction, and photolysis rate effect is dominant. Our study underscores the importance of photolysis rate effect and heterogeneous reactions for O_3, and such interaction processes should be fully considered in future atmospheric chemistry modeling.

Key words: PM, ozone, photolysis, heterogeneous reaction, Nanjing, urban atmosphere

Citation: Qu, Y. W., and Coauthors, 2018: Influence of atmospheric particulate matter on ozone in Nanjing, China: Observational study and mechanistic analysis. *Adv. Atmos. Sci.*, **35**(11), 1381–1395, https://doi.org/10.1007/s00376-018-8027-4.

1. Introduction

Air pollution has become increasingly significant in Nanjing, China, because of its accelerating urbanization and industrialization (Xie et al., 2016; Chen et al., 2017; Zhu et al., 2017). As the major atmospheric pollutants in the urban area, particulate matter (PM) and ozone (O_3) have drawn much attention in recent years for their adverse effects on human health (Kan et al., 2008; Xie et al., 2017). Particles and O_3 are short-lived and radiatively active chemicals (Liao et al., 2015; Park et al., 2016). The chemical interaction between O_3 and PM is complicated. O_3 is believed to have an influence on PM concentrations. O_3 can act as an oxidant, as well as have an impact on the concentration of hydroxyl (OH) radicals and affect the formation of sulfate (SO_4^{2-}), nitrate (NO_3^-), ammonium (NH_4^+), secondary organic aerosols, etc. (Yang et al., 2014; Shi et al., 2015; Li et al., 2017). PM can strengthen the extinction capacity of the atmosphere directly, and it can also act as the cloud condensation nuclei that influence radiation indirectly through affecting cloud formation. Therefore, PM can influence the photolysis rate of O_3 and its precursors by changing solar radiation (Cai et al., 2013; Nishanth et al., 2014; Xie et al., 2014). PM can also influence the transportation and diffusion of O_3 and its precursors through changing the atmospheric stability (Chan et al., 1999; Velasco et al., 2008; Qu et al., 2017). Moreover, the heterogeneous reactions of chemicals, such as NO_x and dinitrogen pentoxide (N_2O_5), on particle surfaces, also exert important influences on the generation and consumption of O_3 (Jacob, 2000; Lou

---

* Corresponding author: Tijian WANG
Email: tjwang@nju.edu.cn

et al., 2014; Akimoto, 2016). However, the mechanism and combined effect of particles on both photolysis rates and heterogeneous reactions are not fully understood.

One of the important pathways through which PM can influence O_3 is by altering the photolysis rate. The scattering and absorbing effect of PM can change the optical properties of the atmosphere and have an impact on the solar radiation that reaches the ground, leading to O_3 variation through altering the photolysis rate and photochemical reactions (Meng et al., 1997; Nishanth et al., 2014). Existing studies generally agree that a reduction in O_3 concentration and productivity is closely related to serious atmospheric PM pollution. Liao et al. (1999) used a radiation transfer model, DISORT, to analyze the impact of aerosols on photochemistry. Tie et al. (2001, 2005) assessed the effects of aerosols on tropospheric oxidants by using a three-dimensional global chemical/transport aerosol model, MOZART, in which photochemical reactions were implemented. They found that surface absorbent particles reduced the photolysis rates and therefore weakened O_3 generation and accumulation, while scattering aerosols did the opposite. Deng et al. (2008, 2011, 2012) compared observations with box model results and analyzed the correlation between PM_{10} (PM with diameters between 2.5 and 10 μm), $PM_{2.5}$ (PM with diameters of 2.5 μm or smaller), O_3, and aerosol optical depth (AOD), in Guangzhou, China. The correlation coefficient between AOD and PM_{10} mass concentration was very high, with a maximum of 0.98, and the AOD and UV radiation/O_3 was anti-correlated, with a correlation coefficient of 0.90. Li et al. (2011a) used a regional chemical transport model coupled with a radiative transfer model to examine the effects of PM on photochemistry in central East China. They found that summertime O_3 in the boundary layer (below 1 km and 1–3 km) was reduced by 5%, with a maximum of 9%, in highly polluted regions.

Heterogeneous reactions on the surface of $PM_{2.5}$ can also affect the concentration of O_3 and secondary particles. Ravishankara (1997) described the role, rates and media of heterogeneous and multiphase reactions in the troposphere, and it was clear from their findings that heterogeneous and multiphase chemistry have the potential to alter the composition of the troposphere. Jacob (2000) proposed that heterogeneous reactions have an impact on O_3 concentrations in a number of ways, including the generation and consumption of NO_x, N_2O_5, HO_x [OH + hydroperoxyl (HO_2)] and O_3, and the generation of halogen radicals. Moreover, according to previous studies (Remorov et al., 2002; Hoffman et al., 2003; Bauer et al., 2004; McNaughton et al., 2009), heterogeneous reactions on the surface of sea salt and soot have significant effects on trace gases. Heterogeneous reactions can also be accelerated by black carbon (BC), which is mainly composed of $PM_{2.5}$ and has a relatively large surface area, leading to changes in the concentrations of gases and particles (Kleffmann and Wiesen, 2005; Kaiser et al., 2011). Deng et al. (2010) applied a box model to study the interactions between aerosols and O_3. Their results showed that the impact of heterogeneous reactions strongly depends on the aerosol concentration and the surface uptake coefficients.

Only a few studies have taken into account the impact of PM on both photochemical and heterogeneous reactions, and were limited to modeling and large-scale observation (Tie et al., 2001, 2005; Bian et al., 2003; Lou et al., 2014). In contrast, the present paper focuses mainly on the mechanism of the impact of PM on O_3 generation and consumption in Nanjing, China. By using field observational data and box modeling, we investigate how PM influences O_3 concentrations through two ways—altering the photolysis rate and affecting heterogeneous reactions on particle surfaces. Section 2 describes the observational data and the box model. The observational data in Nanjing for the whole of 2008 and a typical case are analyzed in section 3. In section 4, we discuss the variations of O_3 and its precursors and secondary aerosols based on the results from a set of sensitivity experiments, in which we consider the impact of PM on photolysis rates and heterogeneous reactions. Finally, conclusions and perspectives on future work are given in section 5.

2. Methods

2.1. *Observation*

The measurement data used in this study were collected at two stations. The first of these was Pukou (PK) air monitoring station (32°18′N, 118°47′E), on Pukou Campus of Nanjing University, in the northwest suburbs of Nanjing. The Industrial Development Zone along the Yangtze River is about 6 km to the northeast of Pukou, and thus this site can be regarded as an industrially polluted suburb. The second one was Caochangmen (CCM) station (32°18′N, 118°26′E), which is located in the urban district and more influenced by human activities. The locations of PK and CCM are shown on the map of Nanjing in Fig. 1. Chemical species are monitored continuously by instruments including an O_3 analyzer (O342M, Environment S. A., Paris, France) for O_3, an ammonia (NH_3) and NO_x analyzer (AC32M-CNH3, Environment S. A., Paris, France) for NO_x, and a PM analyzer (MP101M, Environment S. A., Paris, France) for PM. The analyzers were calibrated daily and observations carried out continuously from October 2007 to August 2009. AOD retrievals were collected from sunphotometer AOD measurements at the Nanjing University of Information Science & Technology site (32.2°N, 118.72°E) of NASA's Stennis Aerosol Robotic Network. In this paper, $PM_{2.5}$, O_3, NO_x and AOD data collected from 1 January to 31 December 2008 are analyzed.

2.2. *Box model*

A zero-dimensional box model, which includes the calculation of aerosol optical properties, UV radiation transmission processes, atmospheric photochemical processes, heterogeneous chemical processes, and aerosol thermodynamic equilibrium processes, was constructed and used in this study.

The OPAC (Optical Properties of Aerosols and Clouds) software package, developed by the University of Munich, Germany, and the Max Planck Institute of Meteorology (Hess

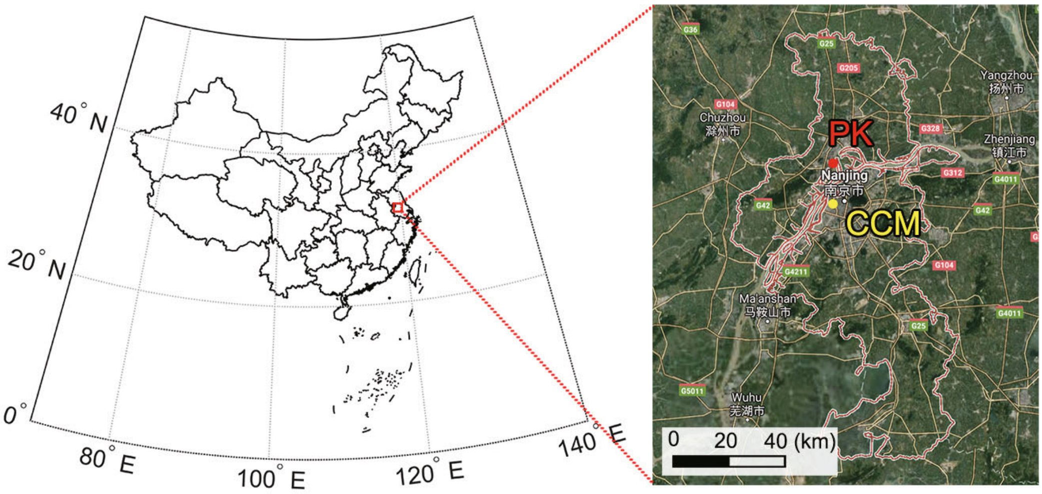

Fig. 1. Map of Nanjing, China, and the locations of the observational sites of Pukou (PK, 32°18′N, 118°47′E) and Caochangmen (CCM, 32°18′N, 118°26′E).

et al., 1998), was used as the optical property module. It provides optical properties including extinction, scattering and absorption coefficients, single scattering albedo (SSA), asymmetry parameter, and phase function. These aerosol optical properties are given for up to 61 wavelengths between 0.25 and 40 μm and eight values of relative humidity. For further details of the OPAC database, please refer to Hess et al. (1998). The UV radiation transmission module was the Tropospheric Ultraviolet and Visible (TUV) radiation model from the National Center for Atmospheric Research (Madronich et al., 1999). TUV was used for calculating the spectral irradiance, spectral actinic flux, and photodissociation coefficients, over the wavelength range 121–750 nm. The carbon bond chemical mechanism known as CB05 (Yarwood et al., 2005) was applied for the photochemical reactions. This mechanism is a comprehensive upgrade of the CB-IV carbon bond mechanism and contains 51 species and 156 reactions (including 23 photolysis reactions). The aerosol chemistry module was the balancing module known as ISORROPIA, developed by Nenes et al. (1998). This module describes the equilibrium of different phase species, including NH_3, hydrogen chloride, nitric acid (HNO_3) gas, solid and liquid SO_4^{2-}, NO_3^-, NH_4^+ and chloride. The heterogeneous chemistry module contains ten reactions, four of which occur on the surface of aqueous aerosols (Jacob, 2000), and the others on BC surfaces (Deng et al., 2010). The first-order rate constant k for heterogeneous loss of a gas to the aerosol is given by

$$k=\left(\frac{r}{D_{\mathrm{g}}}+\frac{4}{m\gamma}\right)^{-1}A\,, \tag{1}$$

in which r is the particle radius, D_{g} is the gas-phase molecular diffusion coefficient of species X in air, m is the mean molecular speed of X in the gas phase, γ is the absorption coefficient on particles, and A is the aerosol surface area per unit volume of air (Jacob, 2000). Heterogeneous reactions and uptake coefficients on BC and aqueous aerosols are listed in Table 1.

Table 1. Heterogeneous reactions and uptake coefficients on BC (Deng et al., 2010) and aqueous aerosols (Jacob, 2000).

	Reactions	Γ
OH	$OH(g)\xrightarrow{BC}OH(ads)$	0.1
HO_2	$HO_2(g)\xrightarrow{\text{aqueous aerosols}}0.5H_2O_2(g)$	0.2
	$HO_2(g)\xrightarrow{BC}HO_2(ads)$	0.1
H_2O_2	$H_2O_2(g)\xrightarrow{BC}H_2O_2(ads)$	1.0×10^{-4}
O_3	$O_3(g)\xrightarrow{BC}O_3(ads)\xrightarrow{BC}O_2(g)$	4.5×10^{-5}
SO_2	$SO_2(g)\xrightarrow{BC}SO_2(ads)\xrightarrow{BC}SO_4^{2-}(c)$	1.0×10^{-5}
NO_2	$NO_2(g)\xrightarrow{\text{aqueous aerosols}}0.5HONO(g)+0.5HNO_3(g)$	1.0×10^{-4}
	$NO_2(g)\xrightarrow{BC}NO_2(ads)\xrightarrow{BC}NO_3^-(c)$	1.0×10^{-4}
NO_3	$NO_3(g)\xrightarrow{\text{aqueous aerosols}}HNO_3(g)$	1.0×10^{-3}
	$NO_3(g)\xrightarrow{BC}NO_3(ads)\xrightarrow{BC}NO_3^-(c)$	5.0×10^{-2}
N_2O_5	$N_2O_5(g)\xrightarrow{\text{aqueous aerosols}}2HNO_3(g)$	0.1
HNO_3	$HNO_3(g)\xrightarrow{BC}HNO_3(ads)\xrightarrow{BC}NO_3^-(c)$	1.0×10^{-3}

The initial $PM_{2.5}$ concentration was set to 105 μg m^{-3}, based on observations. In addition, according to previous works on PM in Nanjing (Wang et al., 2002; Yang et al., 2005; Yin et al., 2009; Chen et al., 2010; Tan et al., 2010), the proportion of PM components was 16% for soluble particles, 25% for SO_4^{2-}, 15% for NO_3^- and NH_4^+, 35% for soluble organic particles, and 9% for BC. All these results were applied as our initial proportion settings. As for size distributions, lognormal distributions were used for each chemical species, more details on which can be found in Hess et al. (1998). The initial NO_x was set to 40 ppb, based on observation in Nanjing. The total volume concentration of volatile organic compounds (VOCs) was 70 ppb at the beginning, and the settings for the proportions of different kinds of VOCs are shown in Table 2 (Liu et al., 2008; Wang and Zhao, 2008). To verify the reasonability of this setup, the SSA was calculated with this box model. The result of 0.76 is close to the SSA observed by Chen et al. (2009), which was 0.75.

3. Observational analysis

3.1. *Statistical characteristics*

Based on hourly data from 1 January to 31 December 2008, the annual mean, standard deviation, median and maximum of $PM_{2.5}$ and O_3 concentrations were calculated, and the results are shown in Table 3. The annual mean and standard deviation values for $PM_{2.5}$ and O_3 at PK station are 94.09 ± 63.42 μg m^{-3} and 16.94 ± 14.91 ppb, respectively. Their counterparts at CCM station are 64.63 ± 47.41 μg m^{-3} and 24.63 ± 22.81 ppb. The $PM_{2.5}$ concentrations at both sites far exceed the national standard concentration, which is 35 μg m^{-3} for the annual mean, according to the China National Ambient Air Quality Standard (China, 2012). Clearly, severe PM pollution exists both in the urban and suburban areas of Nanjing, probably originating from industry, vehicle emissions, and dust blown by winds above unpaved roads (Wang et al., 2012). The PK site shows relatively high $PM_{2.5}$ and low O_3 levels compared with CCM, suggesting severer particulate pollution in the suburbs of Nanjing. One possible explanation is that PK station is situated near an industrial area and has mountains on both its north and southwest side (Shao et al., 2016). The relatively higher levels of industrial emissions and worse diffusion conditions lead to the relatively higher $PM_{2.5}$ concentrations at PK, which may reduce the O_3 concentration.

Table 2. Composition of VOCs and their proportions in the box-model setup. The numbers in the table represent the ratio between the number of functional groups and the number of VOC molecules; therefore, the total percentage is not 100%.

Component	Proportion (%)	Component	Proportion (%)
Carbon–carbon single bond	196.54	Methylbenzene (TOL)	13.79
Carbon–carbon double bond 1 (OLE)	9.00	Xylene (XYL)	4.44
Carbon–carbon double bond 2 (IOLE)	1.66	Ethane (ETHA)	9.08
Methanal (HCHO)	0.44	Ethylene (ETH)	10.66
Other aldehydes (ALD2)	0.39	Isoprene (ISOP)	0.36

Table 3. Statistics (annual mean, median, standard deviation and maximum) of $PM_{2.5}$ (μg m^{-3}) and O_3 (ppb) concentrations from CCM and PK stations in 2008.

	CCM		PK	
	$PM_{2.5}$	O_3	$PM_{2.5}$	O_3
Annual mean	64.6	24.6	94.1	16.9
Median	55.3	16.8	81.9	12.9
Standard deviation	47.4	22.8	63.4	14.9
Maximum	526.7	176.4	558.7	90.5

3.2. *Seasonal variation*

Figure 2 illustrates the seasonal mean $PM_{2.5}$ and O_3 concentrations. The seasonal trends of O_3 are consistent at both sites, with a maximum in spring and minimum in winter. Solar radiation is higher in summer and spring compared with the rest of the year, but a large amount of precipitation in summer—especially during the mei-yu period—reduces the solar radiation and leads to a lower O_3 concentration in summer than in spring (Tong et al., 2017). Therefore, O_3 peaks in spring, with a value of 32.41 ppb and 21.77 ppb at CCM and PK, respectively. The $PM_{2.5}$ concentrations at CCM and PK in spring are 63.15 μg m^{-3} and 92.37 μg m^{-3}, respectively. In summer, the $PM_{2.5}$ concentration reduces to 53.33 μg m^{-3} at CCM but rises to a peak of 119.41 μg m^{-3} at PK. One possible explanation is that most of the factories in Pukou are located to the southeast of PK station. Southeasterly wind, which is the prevailing wind in summer in Nanjing, will bring pollutants from the factories to PK station, leading to the maximum $PM_{2.5}$ (Xiao et al., 2017). The O_3 concentrations in summer are 29.07 ppb and 19.03 ppb at CCM and PK, respectively, and the O_3 concentration in autumn is similar to that in summer. In autumn, the $PM_{2.5}$ concentrations are 73.01 μg m^{-3} and 91.27 μg m^{-3} at CCM and PK, respectively. The $PM_{2.5}$ concentrations in winter are 77.87 μg m^{-3} at CCM and 86.15 μg m^{-3} at PK, and the O_3 concentrations at the two stations are both around 17 ppb. Comparing the two sites, regardless of season, lower O_3 concentrations will be accompanied by higher PM. O_3 concentrations are lower at PK than at CCM in all four seasons; whereas, $PM_{2.5}$ at PK is higher than that at CCM in each season. This phenomenon may be linked to the inverse relationship between $PM_{2.5}$ and O_3.

3.3. *Weekly variation*

The weekly variations of $PM_{2.5}$ and O_3 are demonstrated in Fig. 3. $PM_{2.5}$ concentrations are lower at weekends than on weekdays, possibly because $PM_{2.5}$ is tightly linked with human activity, i.e., the reduced vehicle and factory emissions may be responsible for the low $PM_{2.5}$ levels at weekends. Indeed, this "weekend effect" on $PM_{2.5}$ has been verified by several studies (e.g., Qin et al., 2004; Jeon, 2015). Previous

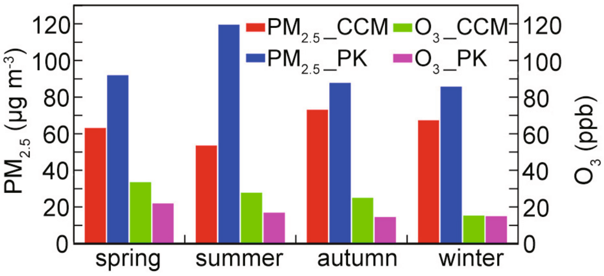

Fig. 2. Seasonal variations of O_3 and $PM_{2.5}$ at CCM and PK stations from 1 January to 31 December 2008.

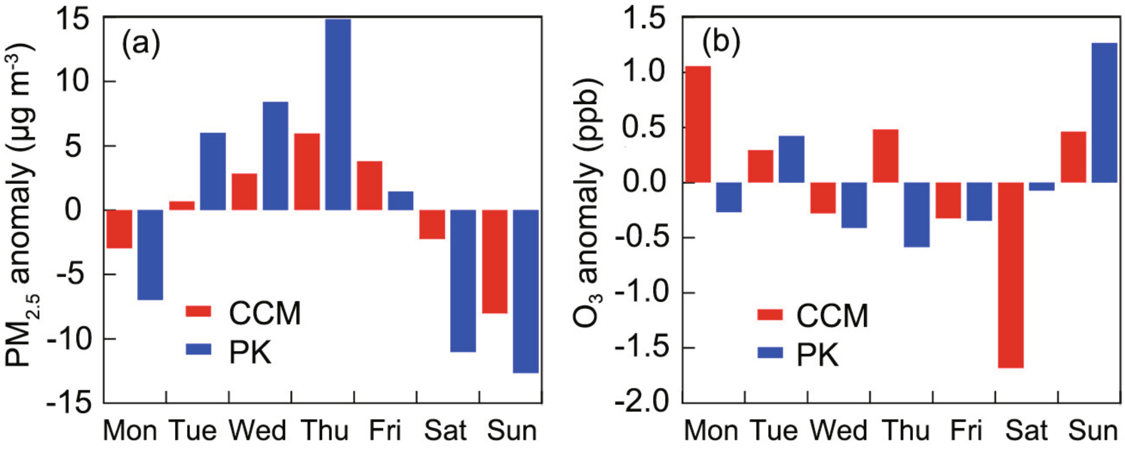

Fig. 3. Weekly cycles of (a) $PM_{2.5}$ and (b) O_3 concentration anomalies at CCM and PK stations from 1 January to 31 December 2008.

studies on O_3 have shown that it is higher at weekends than at other times of the week, which is perhaps attributable to the nonlinear response of O_3 to reduced NO_x concentrations under VOC-sensitive regimes (Heuss et al., 2003; Gao and Niemeier, 2007; Pierce et al., 2010). In our observations, the O_3 "weekend effect" is less significant than that of $PM_{2.5}$, with higher O_3 only observed on Sundays. The weekly variation shows an inverse correlation between $PM_{2.5}$ and O_3. At PK station, $PM_{2.5}$ rises from Monday to Thursday, while O_3 concentrations decline from Tuesday; and when the $PM_{2.5}$ concentration declines from Thursday to Sunday, O_3 shows the opposite trend. Observations at CCM show a similar anti-correlation between $PM_{2.5}$ and O_3 from Monday to Wednesday, as well as at weekends.

3.4. *Daily variation*

Figure 4 depicts the diurnal variations of O_3 and $PM_{2.5}$ in different seasons, which shows an opposite trend between $PM_{2.5}$ and O_3. The latter shows a single-peak pattern at both stations. From the figure, the O_3 concentration is at a minimum in the early morning. Then, due to enhanced atmospheric photochemical activity, O_3 generates and accumulates rapidly before reaching a peak in the afternoon at around 1400 LST (local standard time). The O_3 concentration then declines because of destruction by NO_x during the night. Afternoon maxima and early morning minima have also been found in previous studies (Khoder, 2009; Tong et al., 2017). The strongest diurnal variation of O_3 occurs in spring, and the weakest in winter; plus, the diurnal variation is more significant in the urban district compared with the suburban area.

The diurnal variation of $PM_{2.5}$ shows a double peak, with one peak appearing between 0700 and 0900 LST, and the other one between 1900 and 2200 LST. Essentially, this pattern is due to human activities and planetary boundary layer (PBL) mixing. With the high numbers of vehicles in the morning and evening rush hours, emissions of $PM_{2.5}$ grow. Boogaard et al. (2010) and Dos Santos-Juusela et al. (2013) found that the temporal variation of particle concentrations was higher at locations near to streets. The double-peak pattern is more pronounced at CCM, suggesting that this urban site is more influenced by traffic, whereas the suburban site (i.e., PK) is mainly influenced by industry. The morning $PM_{2.5}$ peak in winter lags that in summer by two hours at PK station. The reason for this phenomenon is that the sun rises around two hours later in the winter (0700 LST) than in summer (0500 LST). Consequently, the morning rush hour and the diffusion of PBL mixing are delayed. During the daytime, stronger solar radiation is beneficial to the development of the PBL. The increased turbulence intensity in the PBL facilitates the diffusion of pollutants, leading to the minimum $PM_{2.5}$ concentration in the afternoon (Qu et al., 2017). The minimum $PM_{2.5}$ appears between 1300 and 1500 LST, during which period the O_3 concentration is usually at its maximum, due to solar radiation and photochemical production.

3.5. *Case study*

Negative correlation between PM and O_3 can be found in all of the variations analyzed above, i.e., seasonal, weekly and daily. In order to eliminate the effects of meteorological conditions, we analyzed a specific case in which there was a steady meteorological field that lasted from 24–30 March 2008 at PK station. Figure 5 shows the time series of meteorological elements including atmospheric pressure, surface temperature, relative humidity, and surface wind velocity. The pressure remains steady from 24–28 March, except for a slightly lower value 26 March. After 29 March, the atmospheric pressure gradually rises to 1020 hPa because of a high-pressure system. The temperature hardly changes during 24–28 March, with the average temperature at around 12° and a maximum of 20°. Surface temperature declines after 29 March. The relative humidity also remains steady during 24–28 March, and then grows to 90% after 29 March because of rain. The wind velocity is less than 8 m s^{-1} during the whole period, except on 28 March when the weather system changes significantly. According to the meteorological conditions, the whole period can be divided into two parts: a steady period

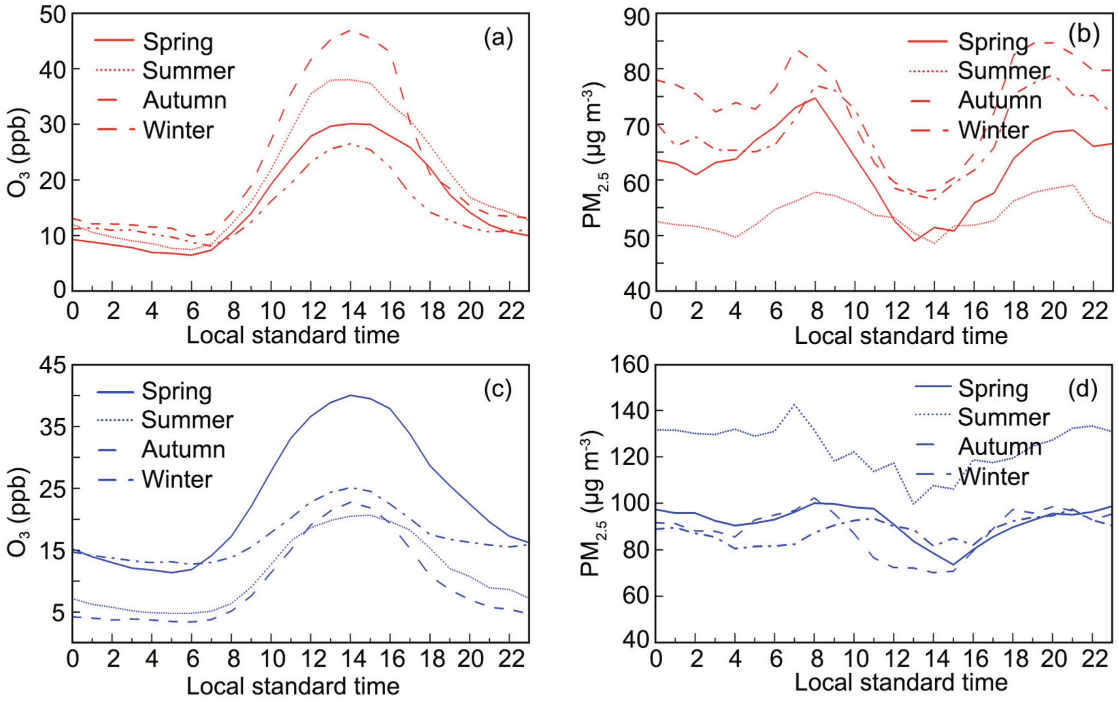

Fig. 4. Diagnal variations of observed (a, c) O_3 and (b, d) $PM_{2.5}$ at (a, b) CCM and (c, d) PK stations in different seasons in 2008.

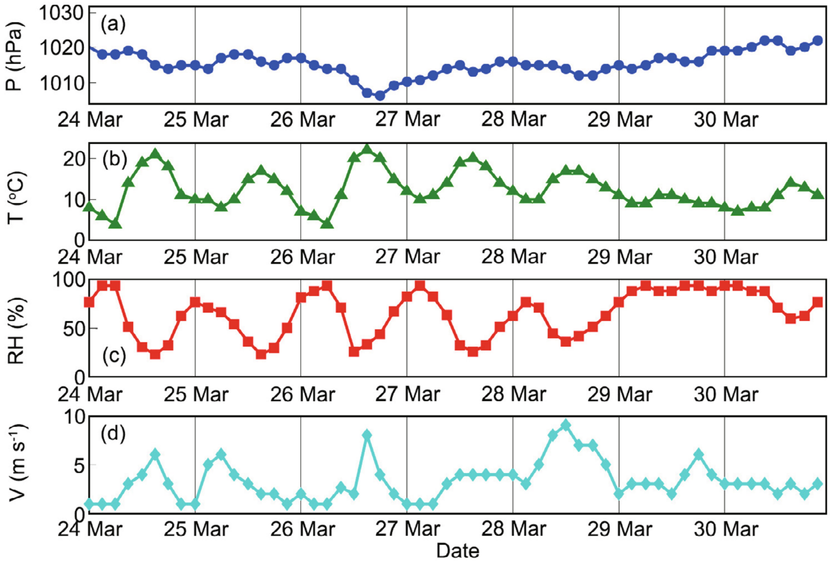

Fig. 5. Observed (a) atmospheric pressure, (b) surface temperature, (c) relative humidity and (d) surface wind velocity at PK station from 29–30 March 2008.

from 24–28 March, and a rainy period from 29–30 March.

Figure 6 shows the time series for $PM_{2.5}$, O_3 and NO_x concentrations, as well as AOD, from 24–30 March 2008 at PK station. The daily average $PM_{2.5}$ rises from 47.3 μg m^{-3} on 24 March to 124.1 μg m^{-3} on 27 March, and the AOD rises by 0.5 (500 nm) and 0.8 (380 nm) in the same period. However, O_3 decreases from 36.7 ppb to 30.7 ppb. On 29 and 30 March, negative correlation between PM and O_3 is apparent, during which time the $PM_{2.5}$ concentration drops dramatically and reaches a minimum at noon on 30 March. Meanwhile, O_3 climbs gradually until 1500 LST 30 March. The negative correlation between PM and O_3 can be observed under the different meteorological conditions of the steady period and rainy period.

To further investigate the negative correlation between $PM_{2.5}$ and O_3, observations on 24 March and 27 March were selected and the hourly concentrations of NO_x, $PM_{2.5}$ and O_3in the daytime (0700–1700 LST) plotted in a scatter dia-

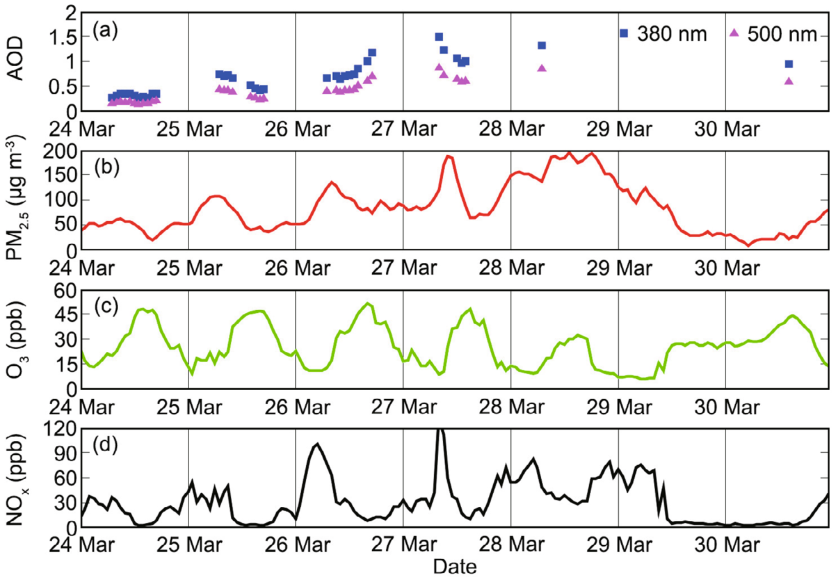

Fig. 6. Observed (a) AOD and (b–d) concentrations of (b) $PM_{2.5}$, (c) O_3 and (d) NO_x in Nanjing from 24–30 March 2008.

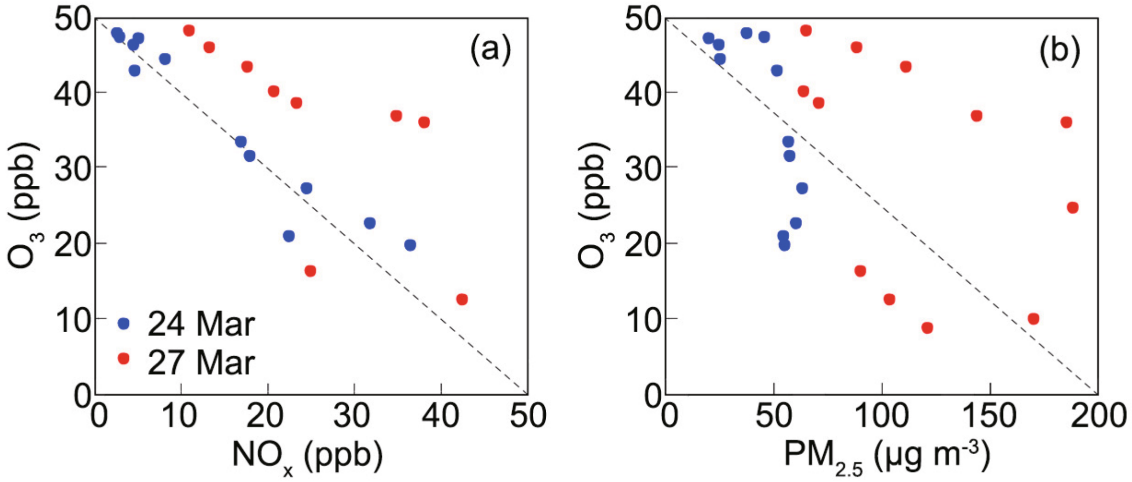

Fig. 7. Relationship between (a) O_3 and NO_x, and (b) O_3 and $PM_{2.5}$, from 24–27 March 2008.

gram (Fig. 7). The opposite relationship between O_3 and NO_x indicates that Nanjing is in a VOC-sensitive region, according to the O_3 isopleths from Empirical Kinetics Modeling Approach (EKMA; Milford et al., 1989; Shiu et al., 2007). An et al. (2015) and Geng et al. (2009) found a similar phenomenon in the Yangtze River Delta region and verified Nanjing as a VOC-sensitive region. The impact of the VOCs/NO_x ratio on PM and O_3 interaction will be discussed later. $PM_{2.5}$ and O_3 concentrations are shown as negatively correlated in Fig. 7. The reason is most likely associated with an enhanced atmospheric PM extinction capacity. An increasing concentration of atmospheric PM (especially fine particles) raises the AOD and weakens the photochemical formation rate of O_3, therefore depressing the O_3 concentration (Li et al., 2011b; Deng et al., 2012; Nishanth et al., 2014). In addition, the particle surface area concentration rises correspondingly when the particle number concentration increases, therefore leading to more heterogeneous reactions taking place on particle surfaces (Deng et al., 2010; Kaiser et al., 2011).

4. Mechanistic analysis

Here, we employ the box model to assess the relative contribution of the photochemical and heterogeneous reactions to the interaction between particles and O_3 under various conditions. The simulation schemes are introduced in section 4.1. Section 4.2 explains the negative correlation between O_3 and PM in the observations at Nanjing. We also run three groups of sensitivity experiments, to investigate the impact of atmospheric scattering capability (section 4.3), particle concentration (section 4.4), and the VOCs/NO_x ratio (section 4.5) on photochemical and heterogeneous reactions.

4.1. *Simulation schemes*

In order to study the impact of particles on photolysis rates and heterogeneous reactions, a set of numerical experiments was designed (Table 4). A control test was carried out without the effect of PM on the photolysis rate or heterogeneous reactions, before the sensitivity runs. A simulation with the effect of aerosols on the photolysis rate but without heterogeneous reactions was set as Case 1. Then, to evaluate the impact of different heterogeneous reactions, four simulations (Case 2-1, 2-2, 2-3 and 2-4), which ignored the effect of aerosols on photolysis, were performed. Case 2-1 only considered heterogeneous reactions of OH, HO_2 and hydrogen peroxide (H_2O_2). Case 2-2 was the same, but with the heterogeneous reaction of O_3 added. Case 2-3 simply included the heterogeneous reaction of nitrogen dioxide (NO_2), whereas Case 2-4 involved the heterogeneous reactions of NO_3^-, dinitrogen pentoxide (N_2O_5) and HNO_3. Next, Case 3-1 and Case 3-2 were designed to investigate the change in photolysis rate in different AOD and SSA scenarios. Compared with Case 3-1, which represented the clean atmosphere, Case 3-2 was a polluted case with the addition of PM. In Case 3-2, the AOD was set as 1 or 2, and the SSA was 1, 0.9 or 0.8. In order to estimate the relative importance of two reactions under different PM concentrations, Case 4, with the effect of PM on photolysis (Case 4-1) and heterogeneous reactions (Case 4-2), was carried out, with the $PM_{2.5}$ concentration varying from 0 to 175 μg m^{-3}. Finally, Case 5 considered photochemical reactions (Case 5-1) and heterogeneous reactions (Case 5-2) with VOCs varying from 0 to 200 ppb and NO_x from 0 to 100 ppb, to compare the impact of particles on O_3 by affecting both kinds of reactions in the O_3–NO_x–VOCs system.

Table 4. Simulation schemes of sensitivity experiments: (a) Control test, Case 1 and Case 2 $(-1,2,3,4)$ applied in studying the impact of PM on O_3 through altering the photolysis rate and heterogeneous reactions; (b) Case 3 $(-1,2)$, Case 4 $(-1,2)$ and Case 5 $(-1,2)$ applied in studying the impact of PM on O_3 under different scenarios, including different AOD and SSA, different $PM_{2.5}$ concentrations, and different VOCs/NO_x regions.

(a)

Test	Photolysis	Heterogeneous reactions			
		OH, HO_2, H_2O_2	O_3	NO_2	NO_3, N_2O_5, HNO_3
Control	-	-	-	-	-
Case 1	√	-	-	-	-
Case 2-1	-	√	-	-	-
Case 2-2	-	-	√	-	-
Case 2-3	-	-	-	√	-
Case 2-4	-	-	-	-	√

(b)

Test	Description
Case 3-1	Clean atmosphere without PM
Case 3-2	Only with impact of PM on photolysis; AOD = 1 or 2; SSA = 1, 0.9 or 0.8
Case 4-1	$PM_{2.5}$ = 0–175 μg m^{-3}; impact of PM on photolysis only
Case 4-2	$PM_{2.5}$ = 0–175 μg m^{-3}; heterogeneous reactions only
Case 5-1	VOCs = 0–200 ppb and NO_x = 0–100 ppb; impact of PM on photolysis only
Case 5-2	VOCs = 0–200 ppb and NO_x = 0–100 ppb; heterogeneous reactions only

In Eq. (2), a variable dX is defined as the deviation between chemical component concentrations in the sensitivity experiments and the control test:

$$\mathrm{d}X_\mathrm{i} = X_\mathrm{i} - X_\mathrm{control}\ . \qquad (2)$$

Here, X_i is the concentration of chemical components in the sensitivity experiments (Case 1–Case 5-2), while X_control is the concentration in the control experiment.

4.2. *Relative importance*

To estimate the relative importance of photochemical reactions and different kinds of heterogeneous reactions to the impact of particles on O_3, with the initial setup based on observational data, the sensitivity experiments including Control, Case 1, and Case 2-1, 2-2, 2-3 and 2-4, are analyzed. Case 1 represents photochemical reactions, and Case 2-1, 2-2, 2-3 and 2-4 were designed to represent the effect of different heterogeneous reactions. The time series of NO_x, HO_x, O_3 and HNO_3 deviations from the control experiment in different case studies are shown in Fig. 8, where dNO_x, dHO_x, dO_3 and dHNO_3 means the deviation of NO_x, HO_x, O_3 and HNO_3, respectively. In Case 1, the average NO_x increases by 19.2 ppb, especially after 12–18 h when the deviation reaches 27.2 ppb. This positive deviation indicates a decline in NO_x consumption. One possible explanation is that the enhancing extinction effects of PM weaken the UV radiation, leading to the reduced photolysis rate. The suppression of NO_x consumption affects the photochemical reactions of O_3, resulting in a 101-ppb reduction in the average O_3 concentration. Due to the weakening of atmospheric oxidation, the HO_x concentration in Case 1 is 30.2 ppt less than in the Control test, and the maximum difference (39.2 ppt) appears after 13 model hours.

Different heterogeneous reactions are taken into account in Case 2-1, 2-2, 2-3 and 2-4. The heterogeneous reactions of H_xO_y (OH + HO_2 + H_2O_2) are added into Case 2-1, and results from the simulation show that the concentration of HO_x radicals in Case 2-1 is 31 ppt less than in the Control test, while NO_x, O_3 and HNO_3 are slightly different in Case 2-1. This indicates that the heterogeneous reaction of H_xO_y is not the main contributor to NO_x photolysis, leading to negligible changes in HNO_3 and O_3 generation. The heterogeneous absorption of O_3 on BC surfaces is considered in Case 2-2. Due to the uptake of O_3, VOC oxidation processes are suppressed and a slight decrease in HO_x can be seen. Case 2-3 simply includes the heterogeneous reaction of NO_2, and a significant change can be observed for all four components. NO_x consumption is accelerated compared with Case 1, and thus the average concentration of precursor-NO_x is reduced by 2.8 ppb, with the largest decline of 22.2 ppb after 4 h. NO_2 transforms into NO_3^- through a heterogeneous reaction, and NO_2

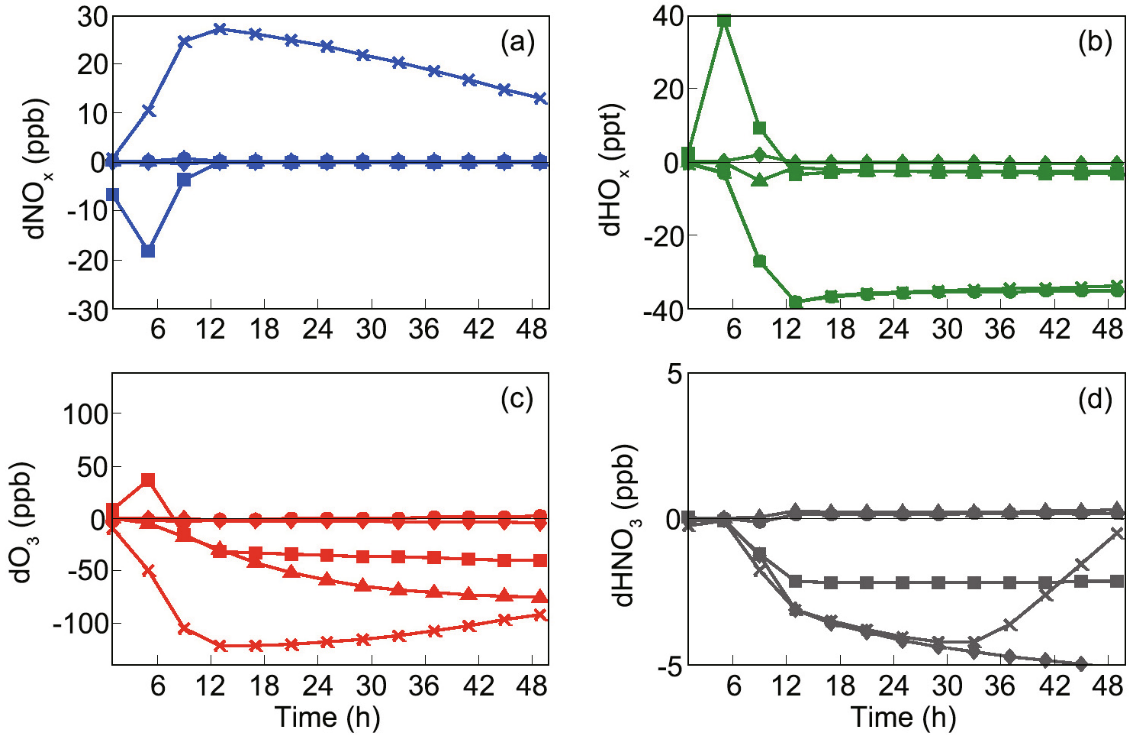

Fig. 8. Variation of (a) dNO_x, (b) dHO_x, (c) dO_3 and (d) $dHNO_3$ in Case 1 to Case 2-4 (crosses represent Case 1; dots represent Case 2-1; triangles represent Case 2-2; squares represent Case 2-3; and diamonds represent Case 2-4).

no longer participates in the generation of O_3 after the transformation. This leads to the phenomenon that O_3 and HO_x concentrations reduce by 36.2 ppb and 2.8 ppt, respectively, after 12 h. However, HO_x and O_3 concentrations rise dramatically at the beginning, which can be explained by the generation of nitrous acid (HONO), which is one of the main products in NO_x heterogeneous reactions. HONO is a significant source of OH in the troposphere (Aumont et al., 2003); therefore, the generation of HONO leads to more HO_x and, subsequently, O_3. Case 2-4 simulates the existence of NO_z (e.g., NO_3, N_2O_5, HNO_3) heterogeneous reactions. Only the average HNO_3 concentration is seen to decrease among the four components. Without considering the effect of aerosols on photolysis rate, NO_3^-, which is generated by the heterogeneous reactions of HNO_3, has little influence on the photolysis reactions of NO_x, HO_x or O_3; thus, the heterogeneous reactions of HNO_3 have negligible impact on NO_x, HO_x and O_3 concentrations.

In this case study, the initial concentration of each species is set based on observations in Nanjing. In Fig. 8c, dO_3 in all of the cases is shown as being negative by the end of the reaction, which demonstrates that O_3 in Nanjing can be reduced by PM through the impact of particles on both photochemical and heterogeneous reactions. Also, this negative correlation is consistent with the observational result. Generally, Case 1 shows a greater reduction in dO_3 than Case 2-1, Case 2-2, Case 2-3 and Case 2-4 combined. This indicates that the effect on photochemical reactions has a greater impact on O_3 than that on heterogeneous reactions. The rate of reduction in Case 1 slows at the end of the 48-h reaction in Fig. 8c. This is possibly because the emissions replenishment mechanism is not taken into consideration in our zero-dimensional box model; therefore, remaining reactants are not as sufficient as at the beginning. Apart from Case 2-1, it is worth noting that the result from Case 2-2 shows the largest reduction in O_3. This demonstrates that the process of O_3 absorption on particle surfaces plays the major role in O_3 depletion among all the heterogeneous reactions.

4.3. *Scattering capability*

In order to understand the impact of atmospheric scattering capability on the photolysis reaction rate, Case 3-1 (clean atmosphere) and Case 3-2 (AOD = 1 or 2 and SSA = 1, 0.9 or 0.8) were simulated. The photolysis rate (J) was calculated by the UV module of the box model, and the profiles of J[NO_2] (the photolysis rate of NO_2) and J[O_3] (the photolysis rate of O_3) in different AOD and SSA scenarios are shown in Fig. 9. According to previous research, surface particles were considered evenly distributed under 2 km in our experiments (Boynard et al., 2014; Petäjä et al., 2016). When calculating the UV radiation, four schemes were set to represent different atmospheric conditions, among which "clean atmosphere" represented the atmosphere without PM. The J[NO_2] and J[O_3] affected by the extinction effect of particles are smaller than those in clean atmospheric conditions near the ground. However, photolysis rates change with height because of different extinction effects of PM. The UV radiation that arrives at the surface will be scattered back into the air by scattering aerosols, enhancing the UV radiation above the aerosol layer. Thus, photolysis rate coefficients in high-

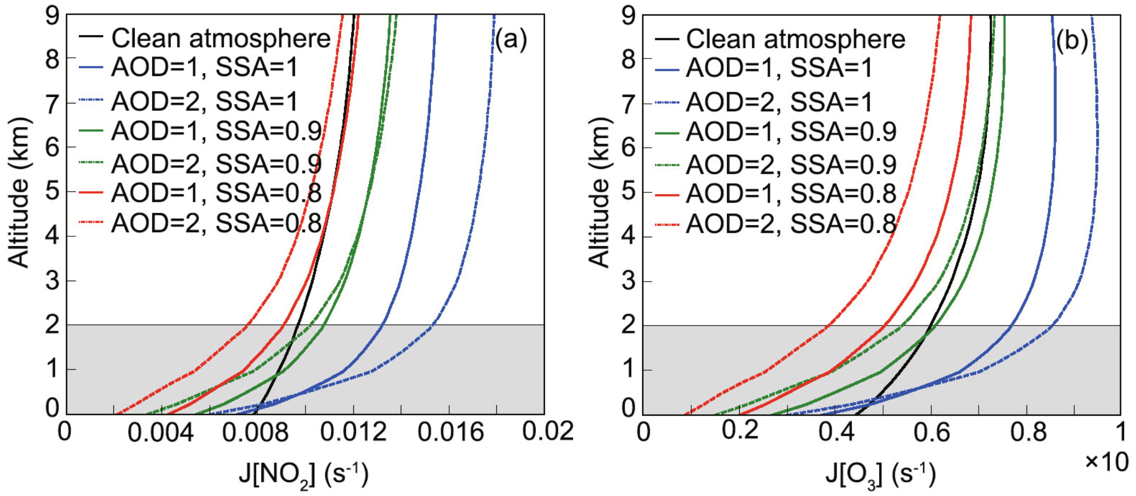

Fig. 9. Photolysis rate profile of (a) NO_2 and (b) O_3 in different AOD and SSA scenarios (Case 3-1 and Case 3-2) in the box-model simulation.

scattering scheme (SSA = 1) elevate correspondingly, and become even larger than in the clean atmosphere scheme. Tie et al. (2005) proposed that absorbent PM (e.g., BC) can reduce the UV radiation both below and above aerosols layers, and this is consistent with our results showing that the diminution of the photolysis rate coefficient occurs at almost all altitudes when SSA = 0.8. In Fig. 9, the effects of scattering and absorbing aerosols are more evident in the case of high AOD. The calculated SSA of all pollutants in Nanjing is relatively low at 0.76; thus, the photolysis rate is reduced in association with the existence of PM.

4.4. *$PM_{2.5}$ concentration*

Sensitivity experiments were carried out to evaluate the relative importance of photochemical and heterogeneous reactions under different PM concentrations. Photochemical (Case 4-1) and heterogeneous reactions (Case 4-2) were compared when the $PM_{2.5}$ concentration changes from 0 to 175 $\mu g\ m^{-3}$, and the variations of NO_x, HO_x, O_3 and HNO_3 in each experiment are shown in Fig. 10. Heterogeneous absorption is strengthened when the PM concentration increases due to the rising surface area of particles, which provides a larger reaction surface. Therefore, dNO_x, dHO_x, dO_3 and $dHNO_3$ in heterogeneous reactions decline with increasing particle concentrations.

The NO_x concentration changes differently under different interaction mechanisms. In Fig. 10a, the photochemical reactions enlarge the NO_x concentration by 0.17 ppb $\mu g^{-1}\ m^3$ on average, while heterogeneous reactions on BC and soluble particle surfaces continue to consume NO_x at a rate of -0.01 ppb $\mu g^{-1}\ m^3$. The photolysis rate decreases because of the extinction effect of PM, and thus the consumption of NO_x slows. The change in HO_x radicals shows a similar trend in two different interactions in Fig. 10b. When the concentration of $PM_{2.5}$ is less than 90 $\mu g\ m^{-3}$, the rate of decline of dHO_x, with consideration of the impact of PM on photochemical reactions, is -0.31 ppt $\mu g^{-1}\ m^3$. The increasing particle concentrations suppress photolysis and affect the atmospheric oxidation, resulting in the declining concentration of HO_x radicals. However, heterogeneous reactions play a more important role in the decline of dHO_x than photolysis under conditions of lower $PM_{2.5}$ levels, with the average rate of change being -0.43 ppt $\mu g^{-1}\ m^3$ when the $PM_{2.5}$ concentration is less than 35 $\mu g\ m^{-3}$. With a rise in the PM concentration, the effects of the two interaction mechanisms tend to be the same. Heterogeneous and photochemical effects on NO_x and HO_x radicals finally result in the reduction of dO_3. In Fig. 10c, the average rates of change of dO_3 affected by both heterogeneous and photochemical reactions are -0.44 ppb $\mu g^{-1}\ m^3$ and -0.71 ppb $\mu g^{-1}\ m^3$, respectively, when $PM_{2.5}$ is under 175 $\mu g\ m^{-3}$. At lower particle concentrations, heterogeneous reactions are the main influence on O_3variation; however, when $PM_{2.5} > 50$ $\mu g\ m^{-3}$, photolysis overtakes heterogeneous reactions and plays the major part in O_3 reduction. In the case study of Nanjing, photochemical reactions are more dominant than heterogeneous reactions for $PM_{2.5} = 105$ $\mu g\ m^{-3}$. In Fig. 10d, $dHNO_3$ rises to a peak of 1 ppb when the $PM_{2.5}$ concentration is 35 $\mu g\ m^{-3}$, after which the change in HNO_3 concentration is similar to that of HO_x radicals. The rates of $dHNO_3$ are -0.03 ppb $\mu g^{-1}\ m^3$ for photochemistry and -0.001 ppb $\mu g^{-1}\ m^3$ for heterogeneous reactions when $PM_{2.5}$ changes from 35 $\mu g\ m^{-3}$ to 175 $\mu g\ m^{-3}$.

4.5. *$VOCs/NO_x$ ratio*

We used a set of sensitivity experiments to verify how O_3 and OH are affected by photochemical (Case 5-1) and heterogeneous reactions (Case 5-2) in the O_3–NO_x–VOCs system, with VOCs varying from 0 to 200 ppb and NO_x from 0 to 100 ppb. Figures 11a and c show dO_3 and dOH as always negative, meaning PM can reduce O_3 and OH through photochemical reactions. This negative effect of particles on O_3 has also been found in other studies. For instance, Li et al. (2011a) reported that surface O_3 was reduced by 5% and OH

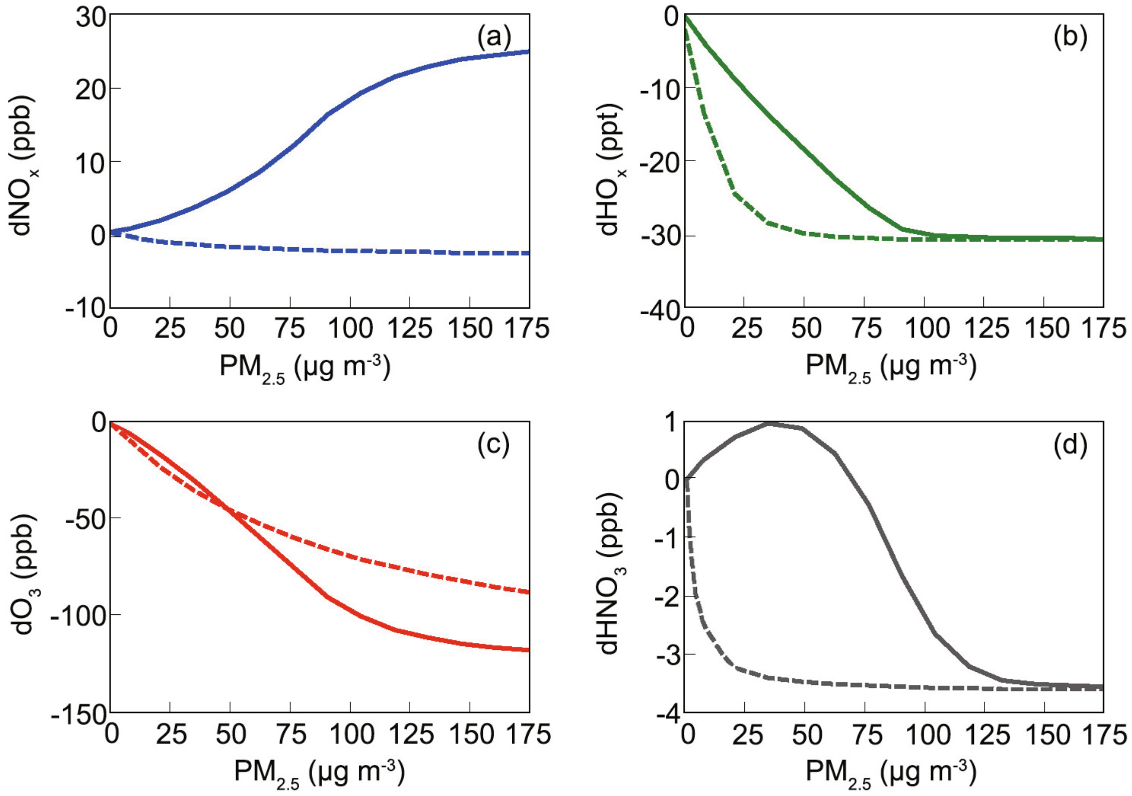

Fig. 10. Variation of (a) dNO_x, (b) dHO_x, (c) dO_3 and (d) $dHNO_3$ in two interaction processes under different $PM_{2.5}$ concentrations. The solid lines represent the photolysis impact process (Case 4-1) and the dashed lines the heterogeneous uptake process (Case 4-2).

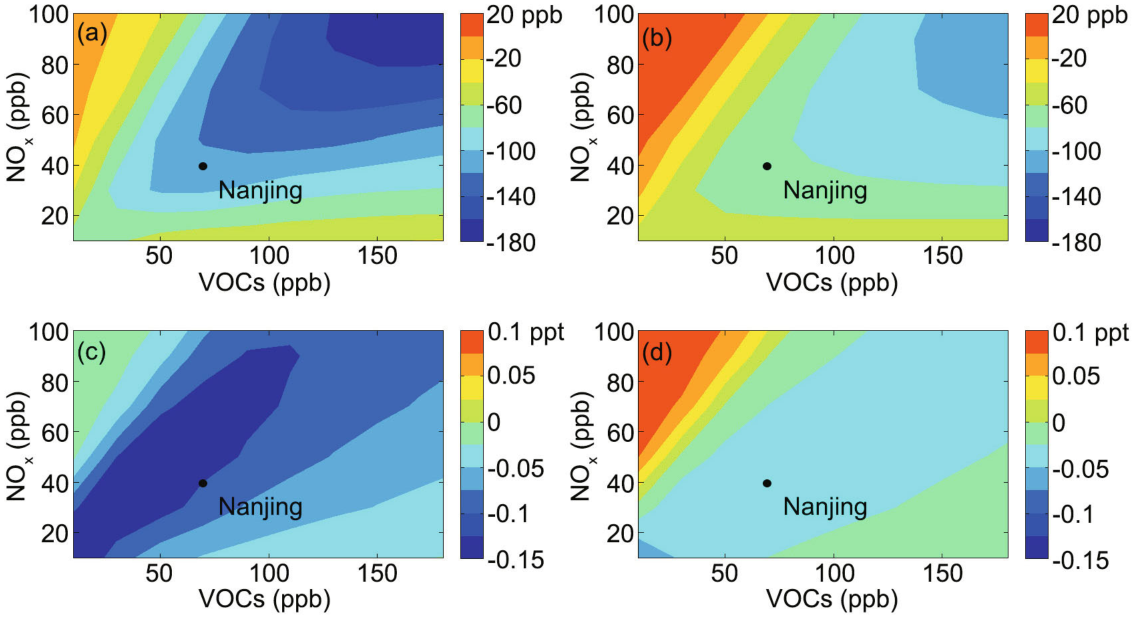

Fig. 11. With varying VOCs/NO$_x$ values (VOCs = 0–200 ppb and NO$_x$ = 0–100 ppb), (a, c) show the changes in dO_3 and dOH when considering photochemical reactions in Case 5-1, and (b, d) show the changes when considering heterogeneous reactions in Case 5-2.

concentrations by 51% via changing photolysis frequencies in central eastern China. Lou et al. (2014) also found a reduction in O_3 when considering the impact of aerosols on O_3 by altering photolysis rates in eastern China. The impact of particles on heterogeneous reactions is illustrated in Figs. 11b and d. Generally, O_3 will be reduced by heterogeneous reactions; however, when NO$_x$ is more than 45 ppb and VOCs less than 60 ppb (VOCs/NO$_x$ ratio of less than 1.33), which represents a typical VOC-sensitive regime, O_3 will increase. This is possibly because excess NO_x will consume O_3 in a VOC-sensitive region (Geng et al., 2009; An et al., 2015). However, when NO_x is consumed by heterogeneous reactions on PM surfaces, the reduction of NO_x limits the consumption of O_3, leading to a rise in the O_3 concentration. According to earlier discussion, Nanjing is a VOC-sensitive region and the initial concentrations of NO_x and VOCs were 40 ppb and 70 ppb, respectively. The VOCs/NO_x ratio of Nanjing is shown in Fig. 11 as a black circle. Although Nanjing is a VOC-sensitive region, the VOCs/NO_x ratio is not low enough to be affected by the increasing effect of heterogeneous reactions in such a region.

Generally, PM reduces O_3 through altering the photolysis rate and heterogeneous reactions. However, O_3 can also be increased by PM in two situations: with a low concentration of particles ($PM_{2.5}$ < 50 µg m^{-3}) and low VOCs/NO_x ratio (< 1.33); and with high PM pollution ($PM_{2.5}$ > 50 µg m^{-3}) and high atmospheric scattering capability. In the case study of Nanjing, the average concentration of $PM_{2.5}$ is larger than 50 µg m^{-3}, according to the observational analysis. Furthermore, the SSA is 0.76 and VOCs/NO_x ratio is 1.75. Thus, particles lead to O_3 reduction through both photochemical and heterogeneous reactions.

5. Conclusions

The interaction between PM and O_3 in Nanjing, in the western part of the Yangtze River Delta region in China, was investigated in this paper through observational analysis and model simulation results.

One year of observations at two sites in 2008 shows that the average concentrations of $PM_{2.5}$ and O_3 are 64.6 ± 47.4 µg m^{-3} and 24.6 ± 22.8 ppb, respectively, for CCM station, and 94.1 ± 63.4 µg m^{-3} and 16.9 ± 14.9 ppb for PK station. A significant diurnal pattern was observed for O_3, with a maximum value in the afternoon and minimum at night; whereas, $PM_{2.5}$ shows a double-peak pattern, with one between 0700 and 0900 LST and the other between 1900 and 2100 LST. Negative correlation between PM and O_3 can be found in the seasonal, weekly and daily variations. In a case study at PK station from 24–27 March 2008, a 6-ppb decrease in O_3 during daytime was found, with an increase in $PM_{2.5}$ by 76.8 µg m^{-3}, along with 0.5 (500 nm) and 0.8 (380 nm) increases in AOD. The correlation coefficient between $PM_{2.5}$ and O_3 reached −0.46.

Previous studies show that the O_3 level is not only affected by the variability of emissions and meteorological conditions, but also chemical processes such as photochemical reactions and heterogeneous reactions (Nishanth et al., 2014; Lou et al., 2014; Akimoto, 2016). The box model simulation in the case study suggests that PM can diminish O_3 through affecting both kinds of reactions, and the effect of photochemical reactions has greater influence than heterogeneous reactions. Of all the heterogeneous reactions considered in this study, the absorption of O_3 on particle surfaces plays the most important role in O_3 reduction.

Modeling results also indicate that the scattering capability of particles has an impact on the rate of photolysis. When SSA = 1, the photolysis rates of J[NO_2] and J[O_3] reach a maximum. On the contrary, when SSA = 0.8, the scattering capability grows weaker and the absorbing capability grows stronger. Consequently, J[NO_2] and J[O_3] decline.

The contribution of aerosol-photolysis and heterogeneous reactions varies depending on the concentration of PM. Heterogeneous reactions play a major role in O_3 destruction at relatively lower particle concentrations ($PM_{2.5}$ < 50 µg m^{-3}), whereas aerosol-photolysis can cause a greater O_3 reduction when the PM concentration is higher ($PM_{2.5}$ > 50 µg m^{-3}). When $PM_{2.5}$ reaches 175 µg m^{-3}, with the impact of aerosols on photochemical reactions, the rate of variation between O_3 and $PM_{2.5}$ concentrations, i.e., $dO_3/dPM_{2.5}$, is −0.71 ppb µg^{-1} m^3. For heterogeneous reactions, the rate is −0.44 ppb µg^{-1} m^3.

Besides the scattering capability and concentration of PM, this study shows that the ratio of VOCs/NO_x can also affect the interactions between PM and O_3. Although particles generally reduce O_3 by their impact on photolysis and heterogeneous reactions, O_3 can, however, be increased by particles through heterogeneous reactions in typical VOC-sensitive regions with low VOCs (< 60 ppb) and high NO_x (> 45 ppb).

In the case study of Nanjing, the SSA is relatively low at 0.76. The annual average concentration of $PM_{2.5}$ is larger than 50 µg m^{-3} and the ratio of VOCs/NO_x is 1.75. Therefore, the effects of both photochemical and heterogeneous reactions lead to O_3 reduction in Nanjing, and the aerosol-photolysis effect plays a major role.

Lastly, we want to emphasize the complexity of the interaction between O_3 and particles. On the one hand, increasing PM enhances the atmospheric extinction capacity and weakens the photochemical formation of O_3. On the other hand, rising particle numbers provide a larger surface area for heterogeneous reactions, thus influencing the O_3 concentration. Our results are acquired based on a short period of observation in Nanjing and zero-dimensional modeling. Clearly, more studies need to be carried out to verify the robustness of our results. Nonetheless, the mechanism revealed in this study, together with other recent research on the interactions between O_3 and PM, should be considered in the chemical module of many climate models. In future work, more simulations based on chemistry models could provide more information to qualify the impact of particles on O_3 generation. In-situ measurements of chemical species and particles are also essential, to evaluate model performance with respect to the interaction mechanisms involved.

Acknowledgements. This work was supported by the National Key Basic Research & Development Program of China (Grant Nos. 2016YFC0203303, 2016YFC0208504 and 2014CB441203), the National Natural Science Foundation of China (Grant Nos. 91544230, 41575145 and 41621005), and the EU 7th Framework Marie Curie Actions IRSES project: REQUA (Grant No. PIRSES-GA-2013-612671).

REFERENCES

Akimoto, H., 2016: Heterogeneous reactions in the atmosphere and uptake coefficients. *Atmospheric Reaction Chemistry*, A. Akimoto, Ed., Springer, pp. 239–284, https://doi.org/10.1007/978-4-431-55870-5_6.

An, J. L., J. N. Zou, J. X. Wang, X. Lin, and B. Zhu, 2015: Differences in ozone photochemical characteristics between the megacity Nanjing and its suburban surroundings, Yangtze River delta, China. *Environmental Science and Pollution Research*, **22**, 19 607–19 617, https://doi.org/10.1007/s11356-015-5177-0.

Aumont, B., F. Chervier, and S. Laval, 2003: Contribution of HONO sources to the NO$_x$/HO$_x$/O$_3$ chemistry in the polluted boundary layer. *Atmos. Environ.*, **37**, 487–498, https://doi.org/10.1016/S1352-2310(02)00920-2.

Bauer, S. E., Y. Balkanski, M. Schulz, D. A. Hauglustaine, and F. Dentener, 2004: Global modeling of heterogeneous chemistry on mineral aerosol surfaces: Influence on tropospheric ozone chemistry and comparison to observations. *J. Geophys. Res.: Atmos.*, **109**(D2), D02304, https://doi.org/10.1029/2003JD003868.

Bian, H. S., M. J. Prather, and T. Takemura, 2003: Tropospheric aerosol impacts on trace gas budgets through photolysis. *J. Geophys. Res.: Atmos.*, **108**(D8), 4242, https://doi.org/10.1029/2002JD002743.

Boogaard, H., D. R. Montagne, A. P. Brandenburg, K. Meliefste, and G. Hoek, 2010: Comparison of short-term exposure to particle number, pm10 and soot concentrations on three (sub) urban locations. *Science of The Total Environment*, **408**, 4403–4411, https://doi.org/10.1016/j.scitotenv.2010.06.022.

Boynard, A., and Coauthors, 2014: First simultaneous space measurements of atmospheric pollutants in the boundary layer from IASI: A case study in the North China Plain. *Geophys. Res. Lett.*, **41**, 645–651, https://doi.org/10.1002/2013GL058333.

Cai, Y., T. J. Wang, M. Xie, and Y. Han, 2013: Impacts of atmospheric particles on surface ozone in Nanjing. *Climatic and Environmental Research*, **18**, 251–260, https://doi.org/10.3878/j.issn.1006-9585.2012.11111. (in Chinese with English abstract)

Chan, Y. C., R. W. Simpson, G. H. McTainsh, P. D. Vowles, D. D. Cohen, and G. M. Bailey, 1999: Source apportionment of visibility degradation problems in Brisbane (Australia) using the multiple linear regression techniques. *Atmos. Environ.*, **33**, 3237–3250, https://doi.org/10.1016/S1352-2310(99)00091-6.

Chen, K., Y. Yin, Y. X. Wei, and W. F. Yang, 2010: Characteristics of carbonaceous aerosols in PM$_{2.5}$ in Nanjing. *China Environmental Science*, **30**, 1015–1020. (in Chinese with English abstract)

Chen, P. L., T. J. Wang, X. B. Lu, Y. Y. Yu, M. Kasoar, M. Xie, and B. L. Zhuang, 2017: Source apportionment of size-fractionated particles during the 2013 Asian Youth Games and the 2014 Youth Olympic Games in Nanjing, China. *Science of the Total Environment*, **579**, 860–870, https://doi.org/10.1016/j.scitotenv.2016.11.014.

Chen, Y., Y. Yin, L. Qian, W. W. Wang, J. D. Yan, C. Chen, 2009: Observation of the absorption and scattering coefficients of atmospheric aerosols in the north suburb of Nanjing from October to December 2007. *Climate and Environmental Research*, **14**, 613–620. (in Chinese with English abstract)

China M. E. P., 2012: Ambient air quality standards. GB 3095-2012. *China Environmental Science Press*.

Deng, J. J., T. J. Wang, L. Liu, and F. Jiang, 2010: Modeling heterogeneous chemical processes on aerosol surface. *Particuology*, **8**, 308–318, https://doi.org/10.1016/j.partic.2009.12.003.

Deng, X. J., and Coauthors, 2008: Effects of Southeast Asia biomass burning on aerosols and ozone concentrations over the Pearl River Delta (PRD) region. *Atmos. Environ.*, **42**, 8493–8501, https://doi.org/10.1016/j.atmosenv.2008.08.013.

Deng, X. J., X. J. Zhou, X. X. Tie, D. Wu, F. Li, H. B. Tan, and T. Deng, 2012: Attenuation of ultraviolet radiation reaching the surface due to atmospheric aerosols in Guangzhou. *Chinese Science Bulletin*, **57**, 2759–2766, https://doi.org/10.1007/s11434-012-5172-5.

Deng, X. J., and Coauthors, 2011: Effect of atmospheric aerosol on surface ozone variation over the Pearl River Delta region. *Science China Earth Sciences*, **54**, 744–752, https://doi.org/10.1007/s11430-011-4172-7.

Dos Santos-Juusela, V., T. Petäjä, A. Kousa, and K. Hämeri, 2013: Spatial-temporal variations of particle number concentrations between a busy street and the urban background. *Atmos. Environ.*, **79**, 324–333, https://doi.org/10.1016/j.atmosenv.2013.05.077.

Gao, H. O., and D. A. Niemeier, 2007: The impact of rush hour traffic and mix on the ozone weekend effect in southern California. *Transportation Research Part D: Transport and Environment*, **12**, 83–98, https://doi.org/10.1016/j.trd.2006.12.001.

Geng, F. H., and Coauthors, 2009: Aircraft measurements of O$_3$, NO$_x$, CO, VOCs, and SO$_2$ in the Yangtze River Delta region. *Atmos. Environ.*, **43**, 584–593, https://doi.org/10.1016/j.atmosenv.2008.10.021.

Hess, M., P. Koepke, and I. Schult, 1998: Optical properties of aerosols and clouds: The software package OPAC. *Bull. Amer. Meteor. Soc.*, **79**, 831–844, https://doi.org/10.1175/1520-0477(1998)079<0831:OPOAAC>2.0.CO;2.

Heuss, J. M., D. F. Kahlbaum, and G. T. Wolff, 2003: Weekday/weekend ozone differences: What can we learn from them? *Journal of the Air & Waste Management Association*, **53**, 772–788, https://doi.org/10.1080/10473289.2003.10466227.

Hoffman, R. C., M. A. Kaleuati, and B. J. Finlayson-Pitts, 2003: Knudsen cell studies of the reaction of gaseous HNO$_3$ with NaCl using less than a single layer of particles at 298 K: A modified mechanism. *J. Phys. Chem. A*, **107**, 7818–7826, https://doi.org/10.1021/jp030611o.

Jacob, D. J., 2000: Heterogeneous chemistry and tropospheric ozone. *Atmos. Environ.*, **34**, 2131–2159, https://doi.org/10.1016/S1352-2310(99)00462-8.

Jeon, B. I., 2015: Characteristics of the springtime weekday/weekend on mass and metallic elements concentrations of PM10 and PM2.5 in Busan. *Journal of Environmental Science International*, **24**, 777–784, https://doi.org/10.5322/JESI.2015.24.6.777.

Kaiser, J. C., N. Riemer, and D. A. Knopf, 2011: Detailed heterogeneous oxidation of soot surfaces in a particle-resolved aerosol model. *Atmospheric Chemistry and Physics*, **11**, 4505–4520, https://doi.org/10.5194/acp-11-4505-2011.

Kan, H. D., S. J. London, G. H. Chen, Y. H. Zhang, G. X. Song, N. Q. Zhao, L. L. Jiang, and B. H. Chen, 2008: Season, sex, age, and education as modifiers of the effects of outdoor air pollution on daily mortality in Shanghai, China: The public health and air pollution in Asia (PAPA) study. *Environmental Health Perspectives*, **116**, 1183–1188, https://doi.org/10.1289/ehp.10851.

Khoder, M. I., 2009: Diurnal, seasonal and weekdays-weekends variations of ground level ozone concentrations in an urban area in greater Cairo. *Environmental Monitoring and Assessment*, **149**, 349–362, https://doi.org/10.1007/s10661-008-0208-7.

Kleffmann, J. and P. Wiesen, 2005: Heterogeneous conversion of NO_2 and NO on HNO_3 treated soot surfaces: Atmospheric implications. *Atmospheric Chemistry and Physics*, **5**, 77–83, https://doi.org/10.5194/acp-5-77-2005.

Li, G., and Coauthors, 2017: A possible pathway for rapid growth of sulfate during haze days in China. *Atmospheric Chemistry and Physics*, **17**, 3301—3316, https://doi.org/10.5194/acp-17-3301-2017.

Li, J., and Coauthors, 2011a: Impacts of aerosols on summertime tropospheric photolysis frequencies and photochemistry over central eastern China. *Atmos. Environ.*, **45**, 1817–1829, https://doi.org/10.1016/j.atmosenv.2011.01.016.

Li, L., and Coauthors, 2011b: Ozone sensitivity analysis with the MM5-CMAQ modeling system for Shanghai. *Journal of Environmental Sciences*, **23**, 1150–1157, https://doi.org/10.1016/S1001-0742(10)60527-X.

Liao, H., W. Y. Chang, and Y. Yang, 2015: Climatic effects of air pollutants over China: A review. *Adv. Atmos. Sci.*, **32**, 115–139, https://doi.org/10.1007/s00376-014-0013-x.

Liao, H., Y. L. Yung, and J. H. Seinfeld, 1999: Effects of aerosols on tropospheric photolysis rates in clear and cloudy atmospheres. *J. Geophys. Res.: Atmos.*, **104**, 23 697–23 707, https://doi.org/10.1029/1999JD900409.

Liu, Y., M. Shao, S. H. Lu, C. C. Liao, J. L. Wang, and G. Chen, 2008: Volatile organic compound (VOC) measurements in the Pearl River Delta (PRD) region, China. *Atmospheric Chemistry and Physics*, **8**, 1531–1545, https://doi.org/10.5194/acp-8-1531-2008.

Lou, S. J., H. Liao, and B. Zhu, 2014: Impacts of aerosols on surface-layer ozone concentrations in China through heterogeneous reactions and changes in photolysis rates. *Atmos. Environ.*, **85**, 123–138, https://doi.org/10.1016/j.atmosenv.2013.12.004.

Madronich, S. and S. Flocke, 1999: The role of solar radiation in atmospheric chemistry. *Environmental Photochemistry. The Handbook of Environmental Chemistry (Reactions and Processes)*, P. Boule, et al., Eds., Springer, pp. 1-26, https://doi.org/10.1007/978-3-540-69044-3_1.

McNaughton, and Coauthors, 2009: Observations of heterogeneous reactions between Asian pollution and mineral dust over the Eastern North Pacific during INTEX-B. *Atmospheric Chemistry and Physics*, **9**, 8283–8308, https://doi.org/10.5194/acp-9-8283-2009.

Meng, Z., D. Dabdub, and J. H. Seinfeld, 1997: Chemical coupling between atmospheric ozone and particulate matter. *Science*, **277**, 116–119, https://doi.org/10.1126/science.277.5322.116.

Milford, J. B., A. G. Russell, and G. J. McRae, 1989: A new approach to photochemical pollution control: implications of spatial patterns in pollutant responses to reductions in nitrogen oxides and reactive organic gas emissions. *Environmental Science & Technology*, **23**, 1290–1301, https://doi.org/10.1021/es00068a017.

Nenes, A., S. N. Pandis, and C. Pilinis, 1998: ISORROPIA: A new thermodynamic equilibrium model for multiphase multicomponent inorganic aerosols. *Aquatic Geochemistry*, **4**, 123–152, https://doi.org/10.1023/A:1009604003981.

Nishanth, T., K. M. Praseed, M. K. S. Kumar, and K. T. Valsaraj, 2014: Influence of ozone precursors and PM_{10} on the variation of surface O_3 over Kannur, India. *Atmospheric Research*, **138**, 112–124, https://doi.org/10.1016/j.atmosres.2013.10.022.

Park, S. S., Y. Jung, and Y. G. Lee, 2016: Spectral dependence on the correction factor of erythemal UV for cloud, aerosol, total ozone, and surface properties: A modeling study. *Adv. Atmos. Sci.* **33**, 865–874, https://doi.org/10.1007/s00376-016-5201-4.

Petäjä, T., and Coauthors, 2016: Enhanced air pollution via aerosol-boundary layer feedback in China. *Scientific Reports*, **6**, 18998, https://doi.org/10.1038/srep18998.

Pierce, T., C. Hogrefe, S. T. Rao, P. S. Porter, and J. Y. Ku, 2010: Dynamic evaluation of a regional air quality model: Assessing the emissions-induced weekly ozone cycle. *Atmos. Environ.*, **44**, 3583–3596, https://doi.org/10.1016/j.atmosenv.2010.05.046.

Qin, Y., G. S. Tonnesen, and Z. Wang, 2004: Weekend/weekday differences of ozone, NO_x, CO, VOCs, PM_{10} and the light scatter during ozone season in southern California. *Atmos. Environ.*, **38**, 3069–3087, https://doi.org/10.1016/j.atmosenv.2004.01.035.

Qu, Y. W., Y. Han, Y. H. Wu, P. Gao, and T. J. Wang, 2017: Study of PBLH and its correlation with particulate matter from one-year observation over Nanjing, Southeast China. *Remote Sensing*, **9**, 668, https://doi.org/10.3390/rs9070668.

Ravishankara, A. R., 1997: Heterogeneous and multiphase chemistry in the troposphere. *Science*, **276**, 1058–1065, https://doi.org/10.1126/science.276.5315.1058.

Remorov, R. G., Y. M. Gershenzon, L. T. Molina, and M. J. Molina, 2002: Kinetics and mechanism of HO_2 uptake on solid NaCl. *J. Phys. Chem. A*, **106**, 4558–4565, https://doi.org/10.1021/jp013179o.

Shao, P., J. L. An, J. Y. Xin, F. K. Wu, J. X. Wang, D. S. Ji, and Y. S. Wang, 2016: Source apportionment of VOCs and the contribution to photochemical ozone formation during summer in the typical industrial area in the Yangtze River Delta, China. *Atmospheric Research*, **176–177**, 64–74, https://doi.org/10.1016/j.atmosres.2016.02.015.

Shi, C. Z., and Coauthors, 2015: A study of aerosol optical properties during ozone pollution episodes in 2013 over Shanghai, China. *Atmospheric Research*, **153**, 235–249, https://doi.org/10.1016/j.atmosres.2014.09.002.

Shiu, C. J., S. C. Liu, C. C. Chang, J. P. Chen, C. C. K. Chou, C. Y. Lin, and C. Y. Young, 2007: Photochemical production of ozone and control strategy for southern Taiwan. *Atmos. Environ.*, **41**, 9324–9340, https://doi.org/10.1016/j.atmosenv.2007.09.014.

Tan, W., and Coauthors, 2010: Analysis of the microphysical characteristics of aerosol particles in clean and pollution area in summer of Nanjing. *Environmental Science rm & Technology*, **33**, 280–286. (in Chinese with English abstract)

Tie, X. X., G. Brasseur, L. Emmons, L. Horowitz, and D. Kinnison, 2001: Effects of aerosols on tropospheric oxidants: A global model study. *J. Geophys. Res.: Atmos.*, **106**, 22 931–22 964, https://doi.org/10.1029/2001JD900206.

Tie, X. X., and Coauthors, 2005: Assessment of the global impact of aerosols on tropospheric oxidants. *J. Geophys. Res.: At-*

mos., **110**, D03204, https://doi.org/10.1029/2004JD005359.

Tong, L., and Coauthors, 2017: Characteristics of surface ozone and nitrogen oxides at urban, suburban and rural sites in Ningbo, China. *Atmospheric Research*, **187**, 57–68, https://doi.org/10.1016/j.atmosres.2016.12.006.

Velasco, E., and Coauthors, 2008: Vertical distribution of ozone and VOCs in the low boundary layer of Mexico City. *Atmospheric Chemistry and Physics*, **8**, 3061–3079, https://doi.org/10.5194/acp-8-3061-2008.

Wang, G. H., L. M. Huang, S. X. Gao, S. T. Gao, and L. S. Wang, 2002: Characterization of water-soluble species of PM_{10} and $PM_{2.5}$ aerosols in urban area in Nanjing, China. *Atmos. Environ*., **36**, 1299–1307, https://doi.org/10.1016/S1352-2310(01)00550-7.

Wang, P., and W. Zhao, 2008: Assessment of ambient volatile organic compounds (VOCs) near major roads in urban Nanjing, China. *Atmospheric Research*, **89**, 289–297, https://doi.org/10.1016/j.atmosres.2008.03.013.

Wang, T. J., and Coauthors, 2012: Urban air quality and regional haze weather forecast for Yangtze River Delta region. *Atmos. Environ*., **58**, 70–83, https://doi.org/10.1016/j.atmosenv.2012.01.014.

Xiao, H., Z. W. Huang, J. J. Zhang, H. L. Zhang, J. S. Chen, H. Zhang, and L. Tong, 2017: Identifying the impacts of climate on the regional transport of haze pollution and intercities correspondence within the Yangtze River Delta. *Environmental Pollution*, **228**, 26–34, https://doi.org/10.1016/j.envpol.2017.05.002.

Xie, M., and Coauthors, 2014: Application of photochemical indicators to evaluate ozone nonlinear chemistry and pollution control countermeasure in China. *Atmos. Environ*., **99**, 466–473, https://doi.org/10.1016/j.atmosenv.2014.10.013.

Xie, M., K. G. Zhu, T. J. Wang, P. L. Chen, Y. Han, S. Li, B. L. Zhuang, and L. Shu, 2016: Temporal characterization and regional contribution to O_3 and NO_x at an urban and a suburban site in Nanjing, China. *Science of the Total Environment*, **551–552**, 533–545, https://doi.org/10.1016/j.scitotenv.2016.02.047.

Xie, M., and Coauthors, 2017: Natural emissions under future climate condition and their effects on surface ozone in the Yangtze River Delta region, China. *Atmos. Environ*., **150**, 162–180, https://doi.org/10.1016/j.atmosenv.2016.11.053.

Yang, H., and Coauthors, 2005: The chemical composition of inorganic and carbonaceous materials in $PM_{2.5}$ in Nanjing, China. *Atmos. Environ*., **39**, 3735–3749, https://doi.org/10.1016/j.atmosenv.2005.03.010.

Yang, Y., H. Liao, and S. J. Lou, 2014: Simulated impacts of sulfate and nitrate aerosol formation on surface-layer ozone concentrations in China. *Atmospheric and Oceanic Science Letters*, **7**, 441–446, https://doi.org/10.1080/16742834.2014.11447204.

Yarwood, G., S. Rao, M. A. Yocke, and G. Z. Whitten, 2005: Updates to the Carbon Bond chemical mechanism: CB05. Final report to the US EPA, RT-04006758.

Yin, Y., Y. Q. Tong, Y. X. Wei, T. J. Wang, J. P. Li, W. F. Yang, and S. X. Fan, 2009: The analysis of chemistry composition of fine-mode particles in Nanjing. *Transactions of Atmospheric Sciences*, **32**, 723–733, https://doi.org/10.3969/j.issn.1674-7097.2009.06.001. (in Chinese with English abstract)

Zhu, K. G., M. Xie, T. J. Wang, J. X. Cai, S. B. Li, W. Feng, 2017: A modeling study on the effect of urban land surface forcing to regional meteorology and air quality over South China. *Atmos. Environ*., **152**, 389–404, https://doi.org/10.1016/j.atmosenv.2016.12.053.